AIP Applied Physics Letters

Role of recombination pathway competition in spatially resolved cathodoluminescence spectroscopy

Milos Toth, Cameron Zachreson, and Igor Aharonovich

Citation: Applied Physics Letters **105**, 241112 (2014); doi: 10.1063/1.4904809
View online: http://dx.doi.org/10.1063/1.4904809
View Table of Contents: http://scitation.aip.org/content/aip/journal/apl/105/24?ver=pdfcov
Published by the AIP Publishing

Articles you may be interested in

Angle-resolved cathodoluminescence spectroscopy
Appl. Phys. Lett. **99**, 143103 (2011); 10.1063/1.3644985

Role of nonradiative recombination centers and extended defects in nonpolar GaN on light emission efficiency
Appl. Phys. Lett. **98**, 072104 (2011); 10.1063/1.3555470

Origin of the excitonic recombinations in hexagonal boron nitride by spatially resolved cathodoluminescence spectroscopy
J. Appl. Phys. **102**, 116102 (2007); 10.1063/1.2821413

Cathodoluminescence versus dynamical epitaxy of Ba -ion irradiated α -quartz
Appl. Phys. Lett. **85**, 1341 (2004); 10.1063/1.1784538

Characterization of silicon dioxide film by high spatial resolution cathodoluminescence spectroscopy
J. Appl. Phys. **92**, 7153 (2002); 10.1063/1.1520726

This article is copyrighted as indicated in the article. Reuse of AIP content is subject to the terms at: http://scitation.aip.org/termsconditions. Downloaded to IP: 138.25.88.80 On: Thu, 05 Feb 2015 02:50:23

CrossMark click for updates

Role of recombination pathway competition in spatially resolved cathodoluminescence spectroscopy

Milos Toth,[a] Cameron Zachreson, and Igor Aharonovich[b]
School of Physics and Advanced Materials, University of Technology, Sydney, 15 Broadway, Ultimo, New South Wales 2007, Australia

(Received 10 November 2014; accepted 7 December 2014; published online 18 December 2014)

Cathodoluminescence (CL) analysis enables characterization of optoelectronic materials and devices with high spatial resolution. However, data interpretation is complicated by the competitive nature of the CL generation process. Specifically, spatially resolved CL profiles are affected by both CL center distributions, and by the unknown distributions of recombination centers that do not generate peaks in measured CL spectra. Here, we use depth-resolved CL to show that the contribution of the latter can be deduced and removed from spatially resolved CL data. The utility of this technique is demonstrated using CL depth profiles of color centers in diamond. © *2014 AIP Publishing LLC*. [http://dx.doi.org/10.1063/1.4904809]

Cathodoluminescence (CL) is a contactless spectroscopic technique based on the detection of infra red (IR), visible, and ultra violet (UV) luminescence excited by energetic electrons.[1,2] CL is typically performed using the focused beam of an electron microscope (Fig. 1(a)), enabling localized spectroscopy and imaging with high spatial and temporal resolution.[3] Applications include characterization of bulk[4–6] and low-dimensional semiconductors,[3,7–11] single photon emitters,[12] photonic cavity resonances,[13] light emitting diodes,[14,15] and plasmonic nanostructures.[16,17] An attractive feature of spatially resolved CL is the ability to depth-profile[1,10,18] materials[19–27] and devices[28,29] by collecting spectra as a function of the electron beam energy, E_b, which controls the electron beam penetration range. This is important for many practical applications since the method is non-destructive and can provide depth resolved information on defect distributions in epilayers, and across interfaces, quantum wells, and devices such as light emitting diodes.

The maximum range of kiloelectronvolt electrons in a solid is approximately proportional to $E_b^{\frac{5}{3}}$,[30] and can be varied up to $\sim 10^4$ nm using a standard scanning electron microscope (SEM). E_b can therefore be used to control the maximum CL generation depth, and to measure the depth-distributions of emitters such as defects and buried low-dimensional nanostructures. However, the utility of CL depth profiling is limited by the fact that most carriers bound with an energy lower than E_b can be ionized by the beam, and most excited electrons are promoted into the conduction band. Hence, recombination can proceed through any one of the j allowed pathways in the solid,[18] giving rise to competition (Fig. 1(b)) that affects the intensities of all CL emission peaks. Specifically, the intensity I_j of a CL peak corresponding to recombination pathway j and a recombination rate of K_j electron-hole pairs per unit time is inversely proportional to the total recombination rate in the solid[31]

$$I_j \propto \frac{K_j}{\sum_j K_j}. \tag{1}$$

The sum over j includes recombination pathways that do (k) and those that do not (l) generate emission peaks in measured CL spectra. It can therefore be written as

$$I_j \propto \frac{K_j}{\sum_k K_k + \sum_l K_l}, \tag{2}$$

where l signifies non-radiative pathways (and centers that radiate outside the spectral range of the experimental setup). The intensity of I_j and the corresponding CL depth profile, $I_j(E_b)$, is therefore modulated by $\sum_l K_l(E_b)$, which is typically unknown and can make unambiguous interpretation of CL depth profiles impossible. Here, we show that, to a first approximation, this component of CL depth profiles can be removed using[31]

$$\Lambda_j(E_b) \approx \frac{I_j(E_b)}{\sum_k I_k(E_b)}, \tag{3}$$

where $I_j(E_b)$ are raw CL depth profiles acquired using a constant power ($E_b J_b$, where J_b is the beam current) electron beam,[32] $\Lambda_j(E_b)$ are the corrected depth profiles, and the sum is over two or more emission peaks in the measured CL spectra.

To demonstrate the validity of Eq. (3), we construct a model of the competitive recombination process, as shown schematically in Fig. 1(b). The model is based on equations for the rate of change of concentration of minority carriers excited by the electron beam, $\frac{\partial n_0}{\partial t}$, and of carriers trapped at recombination centers, $\frac{\partial n_j}{\partial t}$

$$\frac{\partial n_0}{\partial t} = \Gamma_0 - n_0 \frac{1}{\tau_0} - \sum_j [\Gamma_j - \Xi_j] + D\nabla^2 n_0, \tag{4}$$

$$\frac{\partial n_j}{\partial t} = \Gamma_j - \Xi_j - n_j \frac{1}{\tau_j}, \tag{5}$$

where $n_0(t, z)$ is the concentration of excess, free, thermalized minority carriers at depth z and time t ($t = 0$ when the electron beam impinges on the solid). $\Gamma_0(z, t)$ is the rate of change of n_0 caused by carrier excitation by the beam, τ_0^{-1} is the free carrier recombination rate, the sum is over all (radiative and

[a]Electronic mail: Milos.Toth@uts.edu.au
[b]Electronic mail: IgorAharonovich@uts.edu.au

This article is copyrighted as indicated in the article. Reuse of AIP content is subject to the terms at: http://scitation.aip.org/termsconditions. Downloaded to IP: 138.25.88.80 On: Thu, 05 Feb 2015 02:50:23

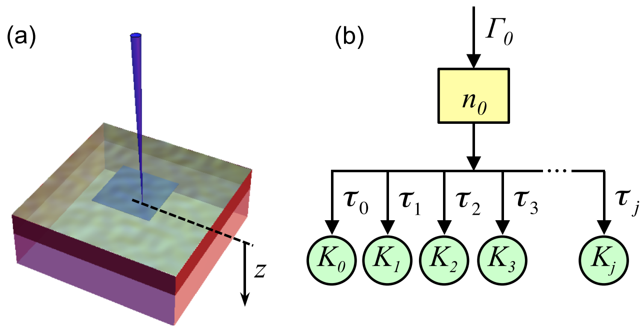

FIG. 1. (a) Schematic illustration of cathodoluminescence generation by a scanned electron beam. (b) Recombination through j pathways in a solid excited by kiloelectronvolt electrons. Each pathway is characterized by a lifetime τ_j and exhibits a recombination rate of K_j electron-hole pairs per unit time (given by Eq. (8)). Γ_0 and n_0 are the minority carrier excitation rate per unit volume (Eq. (6)) and the excess minority carrier concentration (Eq. (4)).

non-radiative) recombination centers j, Γ_j, and Ξ_j are the rates of change of n_0 caused by carrier trapping and de-trapping at recombination center j, respectively, and D is the free carrier diffusion coefficient. Γ_0 can be approximated by[18]

$$\Gamma_0 \approx \frac{1}{E_p}\frac{\partial E}{\partial z} f_b, \tag{6}$$

where E_p is the mean energy that must be deposited into the solid by the electron beam to excite a single electron-hole pair ($E_p \approx 3E_g + 0.5\,\text{eV}$, where E_g is the bandgap[33]), $\frac{\partial E}{\partial z}(z)$ is the electron beam energy deposition depth profile in the solid,[11,34] and f_b is the electron beam flux ($f_b = J_b/A$, where and A is the area irradiated by the beam).

In Eq. (5), $n_j(z,t)$ is the concentration of carriers trapped at center j, and τ_j is the corresponding recombination lifetime. Γ_j is given by[35]

$$\Gamma_j = v_0 n_0 \sigma_j N_j \left(1 - \frac{n_j}{N_j}\right), \tag{7}$$

where v_0 is the free carrier thermal velocity, and $N_j(z)$ and σ_j are the concentration and carrier capture cross-section of center j, respectively. The term in brackets is the fraction of the centers j that are unoccupied (i.e., ionized) at depth z, and limits the concentration of $n_j(z)$ to $N_j(z)$.

Equations (4) and (5) are solved to get $n_0(t, z)$ and $n_j(t,z)$.[34] Electron-hole pair recombination rates in the volume excited by the electron beam are obtained by integrating $n_0(z,t)$ and $n_j(z,t)$ over z

$$K_i \approx A\frac{1}{\tau_i}\int n_i\, dz, \tag{8}$$

where K_0 and $K_{j\geq 1}$ are proportional to the intensities of intrinsic and extrinsic CL emission peaks, respectively ($I_j \propto K_j$). CL depth profiles are therefore simulated by calculating the steady state rates K_0^∞ and K_j^∞ as a function of E_b.[34]

Corrected CL depth profiles, $\Lambda_j(E_b)$, are given by[31]

$$\Lambda_j \approx \frac{K_j^\infty(E_b)}{\sum_k K_k^\infty(E_b)}, \tag{9}$$

where the sum is over all recombination pathways that are assumed to generate peaks detected in CL spectra (i.e., Eq. (9) is equivalent to Eq. (3)). Equation (9) can be applied to both intrinsic ($j = 0$) and extrinsic ($j \geq 1$) CL emissions, provided the former are corrected for self-absorption.[21] Equation (9) (and Eq. (3)) is an approximation in that it operates on CL emission peak intensities, but does not account for the changes in $n_0(z)$ caused by the removal of non-radiative centers from a sample.

The above model enables the simulation of CL depth profiles from a material with arbitrary depth-distributions of j recombination centers. Here, we simulate a 1.5 μm diamond film that contains five defect species ($j = 1$–5) with the depth distributions shown in Fig. 2. Defects 1 and 4 are assumed to be non-radiative, while centers 2, 3, and 5 are assumed to produce emissions that are detected by a CL spectrometer. The model input parameters and selected model outputs are given in the supplementary material.[34]

Fig. 3(a) shows CL depth profiles, $I_j(E_b)$, simulated for the sample shown in Fig. 2. The depth profiles of the radiative centers ($j = 2$, 3, and 5) are substantially different from the corresponding depth distributions $N_2(z)$, $N_3(z)$, and $N_5(z)$ seen in Fig. 2 due to competitive recombination at the non-radiative centers 1 and 4. Fig. 3(b) shows the corrected depth profiles, $\Lambda_j(E_b)$, obtained using Eq. (9). The corrected curves correlate well with the recombination center depth distributions in Fig. 2, indicating the validity of Eq. (9). Specifically, N_3 and Λ_3 do not vary with z, N_2 and Λ_2 decrease with z, and N_5 and Λ_5 increase with z over the range of depths probed by the CL depth profiles (i.e., $z = 0$ to $\sim$700 nm). Differences between the exact shapes of Λ_3 and N_3 (as well as Λ_2 and N_2, and Λ_5 and N_5) are caused primarily by the shapes and finite sizes of the corresponding CL generation functions $\tau_j^{-1} n_j(z)$, and by competition between the three CL centers.

To demonstrate the applicability of the CL correction technique to real samples, we employ a 400 nm nanodiamond film with a grain size of $\sim 250 \pm 50$ nm.[36] The film had been pre-irradiated for 25 min by a 20 keV, high power ($E_b J_b \approx 22$ mW) electron beam in the presence of H_2O adsorbates so as to generate a well-defined distribution of nitrogen-vacancy (NV) luminescence centers. CL depth profiles were acquired using an electron beam power of 5.3 μW

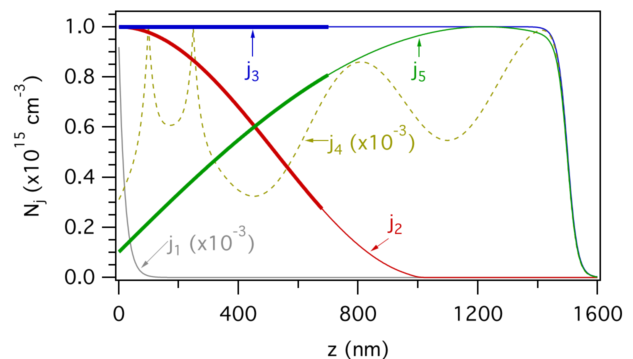

FIG. 2. Recombination center concentrations (N_j) plotted as a function of depth (z) for the five centers ($j = 1$ to 5) considered in the simulations. Thick lines between $z = 0$ and 700 nm show parts of the curves probed by the simulated CL depth profiles shown in Fig. 3.

This article is copyrighted as indicated in the article. Reuse of AIP content is subject to the terms at: http://scitation.aip.org/termsconditions. Downloaded to IP: 138.25.88.80 On: Thu, 05 Feb 2015 02:50:23

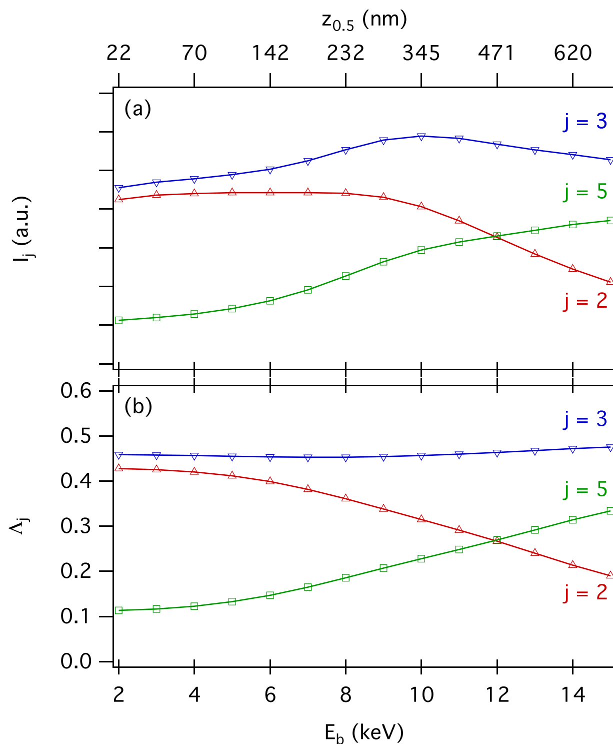

FIG. 3. (a) CL depth profiles simulated for the sample shown in Fig. 2, and (b) the corresponding depth profiles corrected using Eq. (9). [$z_{0.5}$ = depth at which 50% of the electron energy is deposited into the sample at each of the beam energies shown on the bottom axis[34]].

(Ref. 32) from a sample area of $\sim 20\,\mu m^2$ using the experimental setup described in Ref. 36.

Fig. 4(a) shows representative CL spectra collected using beam energies of 2, 5, and 10 keV. The spectra contain NV^0, A-band, and H3 emissions (attributed to charge neutral nitrogen-vacancy defects, dislocations, and nitrogen-vacancy complexes, respectively)[37] which were fit using the method described in Ref. 36. The peak areas, I_j, were used to generate the CL depth profiles shown in Fig. 4(b), and Eq. (3) was applied to these data to generate the corresponding corrected depth profiles, $\Lambda_j(E_b)$, shown in Fig. 4(c).

In this sample, the concentration of NV centers is expected to increase with depth below the diamond surface because:[36] (i) the 20 keV electron beam pre-irradiation treatment activates NV centers through dehydrogenation of NVH_x complexes, and (ii) the activation efficiency increases with distance below the surface of the 400 nm diamond film. However, the raw CL depth profiles (Fig. 4(b)) do not show this trend, likely because they are dominated by the depth-distributions of competing non-radiative defects present in the highly heterogeneous polycrystalline diamond film. Conversely, the corrected depth profiles (Fig. 4(c)) do show the expected increase in NV^0 intensity with E_b. The corrected A-band depth profile shows the opposite trend, and can be attributed either to competition with NV centers or a decrease in the concentration of A-band centers (the latter may be a consequence of electron beam induced etching by residual H_2O adsorbates[36]). The corrected intensity of the weak H3 emission is approximately constant with E_b. The corrected depth profiles in Fig. 4(c) serve as experimental evidence for the validity of Eq. (3). The correction technique

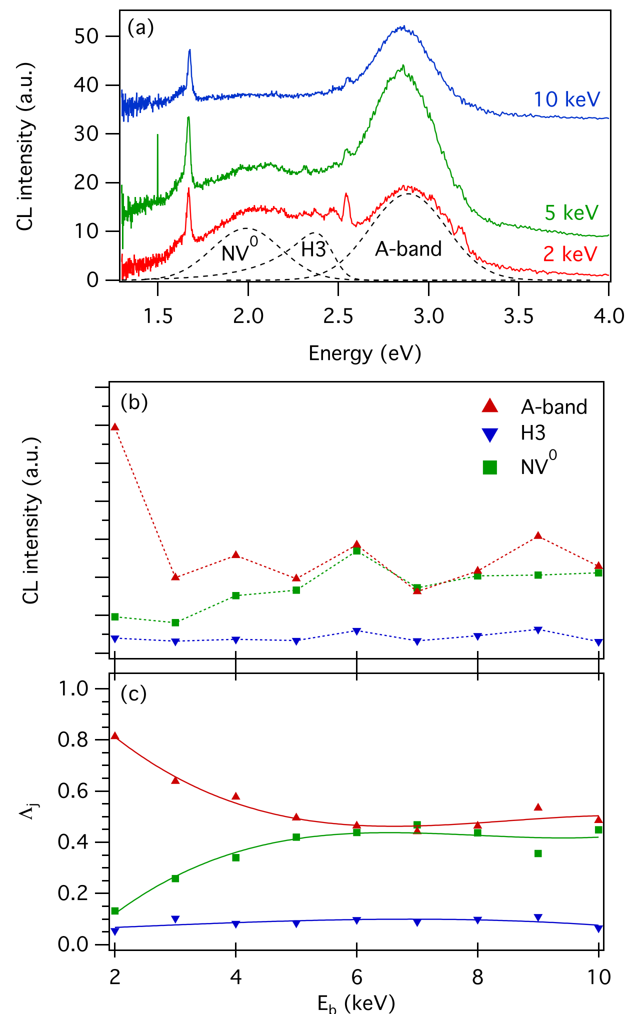

FIG. 4. (a) CL spectra acquired using beam energies of 2, 5, and 10 keV, and the NV^0, H3, and A-band peaks used to fit the 2 keV spectrum. (b) Raw CL depth profiles and (c) the corresponding corrected depth profiles obtained using Eq. (3).

yielded the expected increase in NV^0 intensity with depth, and the remaining profiles were interpreted in terms of the depth distributions and competition between luminescent CL centers.

In conclusion, our modeling and experimental results show that Eq. (3) can be used to correct CL depth profiles for the effects of non-radiative recombination centers (and centers that radiate outside the spectral range of the CL detection system). It can be applied to spatially resolved CL data comprised of two or more emission peaks that had been acquired using a constant power electron beam.

This work was supported by FEI Company and the Australian Research Council (Project No. DP140102721). I.A. is the recipient of an Australian Research Council Discovery Early Career Research Award (Project No. DE130100592).

[1] B. G. Yacobi and D. B. Holt, *Cathodoluminescence Microscopy of Inorganic Solids* (Springer, 1990).
[2] C. M. Parish and P. E. Russell, Adv. Imaging Electron Phys. **147**, 1 (2007).

This article is copyrighted as indicated in the article. Reuse of AIP content is subject to the terms at: http://scitation.aip.org/termsconditions. Downloaded to IP: 138.25.88.80 On: Thu, 05 Feb 2015 02:50:23

[3]M. Merano, S. Sonderegger, A. Crottini, S. Collin, P. Renucci, E. Pelucchi, A. Malko, M. H. Baier, E. Kapon, B. Deveaud, and J. D. Ganière, Nature **438**, 479 (2005).
[4]X. Fu, G. Jacopin, M. Shahmohammadi, R. Liu, M. Benameur, J. D. Ganière, J. Feng, W. Guo, Z. M. Liao, B. Deveaud, and D. Yu, ACS Nano **8**, 3412 (2014).
[5]N. Pauc, M. R. Phillips, V. Aimez, and D. Drouin, Appl. Phys. Lett. **89**, 161905 (2006).
[6]M. Toth, K. Fleischer, and M. R. Phillips, Phys. Rev. B **59**, 1575 (1999).
[7]L. A. Padilha, W. K. Bae, V. I. Klimov, J. M. Pietryga, and R. D. Schaller, Nano Lett. **13**, 925 (2013).
[8]M. Grundmann, J. Christen, N. N. Ledentsov, J. Böhrer, D. Bimberg, S. S. Ruvimov, P. Werner, U. Richter, U. Gösele, J. Heydenreich, V. M. Ustinov, A. Y. Egorov, A. E. Zhukov, P. S. Kop'ev, and Z. I. Alferov, Phys. Rev. Lett. **74**, 4043 (1995).
[9]L. Samuelson and A. Gustafsson, Phys. Rev. Lett. **74**, 2395 (1995).
[10]A. Gustafsson, M. E. Pistol, L. Montelius, and L. Samuelson, J. Appl. Phys. **84**, 1715 (1998).
[11]M. Toth and M. R. Phillips, Scanning **20**, 425 (1998).
[12]L. H. G. Tizei and M. Kociak, Phys. Rev. Lett. **110**, 153604 (2013).
[13]S. Choi, C. Ton-That, M. R. Phillips, and I. Aharonovich, Appl. Phys. Lett. **103**, 171102 (2013).
[14]T. Sekiguchi and S. Koizumi, Appl. Phys. Lett. **81**, 1987 (2002).
[15]B. Chen, J. Chen, T. Sekiguchi, T. Ohyanagi, H. Matsuhata, A. Kinoshita, H. Okumura, and F. Fabbri, Appl. Phys. Lett. **93**, 033514 (2008).
[16]F. J. Garcia de Abajo, Rev. Mod. Phys. **82**, 209 (2010).
[17]T. Coenen, F. B. Arango, A. F. Koenderink, and A. Polman, Nat. Commun. **5**, 3250 (2014).
[18]B. G. Yacobi and D. B. Holt, J. Appl. Phys. **59**, R1 (1986).
[19]K. Fleischer, M. Toth, M. R. Phillips, J. Zou, G. Li, and S. J. Chua, Appl. Phys. Lett. **74**, 1114 (1999).
[20]S. O. Kucheyev, M. Toth, M. R. Phillips, J. S. Williams, C. Jagadish, and G. Li, Appl. Phys. Lett. **78**, 34 (2001).
[21]O. Gelhausen, M. R. Phillips, and M. Toth, J. Appl. Phys. **89**, 3535 (2001).
[22]Y. Dong, Z. Q. Fang, D. C. Look, G. Cantwell, J. Zhang, J. J. Song, and L. J. Brillson, Appl. Phys. Lett. **93**, 072111 (2008).
[23]K. C. Hui, H. C. Ong, P. F. Lee, and J. Y. Dai, Appl. Phys. Lett. **86**, 152116 (2005).
[24]H. C. Ong, A. S. K. Li, and G. T. Du, Appl. Phys. Lett. **78**, 2667 (2001).
[25]J. D. Ye, H. Zhao, W. Liu, S. L. Gu, R. Zhang, Y. D. Zheng, S. T. Tan, X. W. Sun, G. Q. Lo, and K. L. Teo, Appl. Phys. Lett. **92**, 131914 (2008).
[26]B. J. Ryan, D. P. Lowney, M. O. Henry, P. J. McNally, E. McGlynn, K. Jacobs, and L. Considine, Thin Solid Films **473**, 308 (2005).
[27]S. Suihkonen, H. Nykänen, T. Tanikawa, M. Yamaguchi, Y. Honda, and H. Amano, Phys. Status Solidi A **210**, 383 (2013).
[28]Z. H. Wu, A. M. Fischer, F. A. Ponce, W. Lee, J. H. Ryou, J. Limb, D. Yoo, and R. D. Dupuis, Appl. Phys. Lett. **91**, 041915 (2007).
[29]Y. Xia, Y. Li, T. Detchprohm, and C. Wetzel, Phys. B: Condens. Matter **404**, 4899 (2009).
[30]K. Kanaya and S. Okayama, J. Phys. D **5**, 43 (1972).
[31]Equations (1)–(3) and (9) are valid if spatially-resolved CL profiles are acquired using a constant power electron beam[32] and recombination center saturation is negligible.
[32]CL depth profiling is typically performed using a constant power ($E_b J_b$) electron beam (where E_b and J_b are the electron beam energy and current, respectively), because the electron-hole pair generation rate is approximately proportional to $E_b J_b$.[1,2,11,18]
[33]R. C. Alig and S. Bloom, Phys. Rev. Lett. **35**, 1522 (1975).
[34]See supplementary material at http://dx.doi.org/10.1063/1.4904809 for a detailed description of model inputs and outputs.
[35]J. G. Simmons and G. W. Taylor, Phys. Rev. B **4**, 502 (1971).
[36]C. Zachreson, A. A. Martin, I. Aharonovich, and M. Toth, ACS Appl. Mater. Interfaces **6**, 10367 (2014).
[37]A. M. Zaitsev, *Optical Properties of Diamond: A Data Handbook* (Springer, 2001).

This article is copyrighted as indicated in the article. Reuse of AIP content is subject to the terms at: http://scitation.aip.org/termsconditions. Downloaded to IP: 138.25.88.80 On: Thu, 05 Feb 2015 02:50:23